THE JOURNAL OF BIOLOGICAL CHEMISTRY VOL. 283, NO. 21, pp. 14461–14468, May 23, 2008
Printed in the U.S.A.

Ca^{2+}-stimulated Basal Adenylyl Cyclase Activity Localization in Membrane Lipid Microdomains of Cardiac Sinoatrial Nodal Pacemaker Cells*[S]

Received for publication, September 10, 2007, and in revised form, March 5, 2008 Published, JBC Papers in Press, March 20, 2008, DOI 10.1074/jbc.M707540200

Antoine Younes[‡1], Alexey E. Lyashkov[‡1], David Graham[§1], Anna Sheydina[‡1], Maria V. Volkova[‡1], Megan Mitsak[§], Tatiana M. Vinogradova[‡], Yevgeniya O. Lukyanenko[‡], Yue Li[‡], Abdul M. Ruknudin[‡], Kenneth R. Boheler[‡], Jennifer van Eyk[§], and Edward G. Lakatta[‡2]

From the [‡]Laboratory of Cardiovascular Science, Gerontology Research Center, NIA, Intramural Research Program, National Institutes of Health, Baltimore, Maryland 21224 and the [§]Department of Medicine, Johns Hopkins University, Baltimore, Maryland 21224

Spontaneous, rhythmic subsarcolemmal local Ca^{2+} releases driven by cAMP-mediated, protein kinase A (PKA)-dependent phosphorylation are crucial for normal pacemaker function of sinoatrial nodal cells (SANC). Because local Ca^{2+} releases occur beneath the cell surface membrane, near to where adenylyl cyclases (ACs) reside, we hypothesized that the dual Ca^{2+} and cAMP/PKA regulatory components of automaticity are coupled via Ca^{2+} activation of AC activity within membrane microdomains. Here we show by quantitative reverse transcriptase PCR that SANC express Ca^{2+}-activated AC isoforms 1 and 8, in addition to AC type 2, 5, and 6 transcripts. Immunolabeling of cell fractions, isolated by sucrose gradient ultracentrifugation, confirmed that ACs localize to membrane lipid microdomains. AC activity within these lipid microdomains is activated by Ca^{2+} over the entire physiological Ca^{2+} range. In intact SANC, the high basal AC activity produces a high level of cAMP that is further elevated by phosphodiesterase inhibition. cAMP and cAMP-mediated PKA-dependent activation of ion channels and Ca^{2+} cycling proteins drive sarcoplasmic reticulum Ca^{2+} releases, which, in turn, activate ACs. This feed forward "fail safe" system, kept in check by a high basal phosphodiesterase activity, is central to the generation of normal rhythmic, spontaneous action potentials by pacemaker cells.

Numerous studies over the past decade have indicated that intracellular Ca^{2+} release is a key feature of normal cardiac pacemaker cell automaticity (1). More recently it has been demonstrated that the basal level of global cAMP in rabbit sinoatrial nodal cells (SANC)[3] exceeds that in ventricular myocytes (2). The high basal cAMP in SANC mediates robust basal protein kinase A (PKA)-dependent phosphorylation of specific surface membrane ion channels and Ca^{2+} cycling proteins, which regulates the periodicity and amplitude of spontaneous, sarcoplasmic reticulum generated, local Ca^{2+} releases in the absence of cell Ca^{2+} overload (2). Local Ca^{2+} releases emanate from ryanodine receptors of sarcoplasmic reticulum that lies beneath the sarcolemma (10–15 nm), near the Na/Ca exchanger (NCX) proteins (3). Local Ca^{2+} releases occur mainly during the late part of the spontaneous diastolic depolarization and activate an inward NCX current (4–7). This imparts an exponential character to the late diastolic depolarization (5, 8, 9), facilitating the achievement of the threshold for opening of L-type Ca^{2+} channels, which generate the rapid upstroke of the subsequent action potential (AP). Thus, cAMP-mediated, PKA-dependent phosphorylation of surface membrane ion channels and SR Ca^{2+} cycling proteins control the SANC basal spontaneous rhythmic firing (2).

The mechanisms that underlie a high basal cAMP in SANC are unknown. The failure of β_1 or β_2 adrenergic receptor (β-AR) inverse agonists to alter the spontaneous, basal SANC firing rate indicates that high levels of cAMP are not due to constitutively active β-ARs (2). Although a reduction in phosphodiesterase (PDE) activity could, in part, account for elevated cAMP levels in SANC, recent evidence suggests that basal PDE activity of SANC is not reduced, but rather, appears to be elevated (10). Moreover, inhibition of basal adenylyl cyclase (AC) activity in SANC substantially reduces cAMP and cAMP-mediated, PKA-dependent phosphorylation of phospholamban (2) suggesting a high constitutive (basal) level of AC activity. Whereas there is some evidence to indicate that SANC harbor Ca^{2+}-activated AC isoforms (11, 12), direct evidence for Ca^{2+} activation of AC activity, and the specific cell microdomains in which this may occur, are lacking. Using multiple approaches we show that both Ca^{2+}-regulated ACs reside in lipid microdomains and that Ca^{2+} activation of AC activity occurs within these domains.

* This work was supported, in whole or in part, by the National Institutes of Health Intramural Research Program, NIA. The costs of publication of this article were defrayed in part by the payment of page charges. This article must therefore be hereby marked "*advertisement*" in accordance with 18 U.S.C. Section 1734 solely to indicate this fact.

[S] The on-line version of this article (available at http://www.jbc.org) contains supplemental Figs. S1–S3 and Tables S1 and S2.

[1] These authors contributed equally to this work.

[2] To whom correspondence should be addressed: Gerontology Research Center, 5600 Nathan Shock Dr., Baltimore, MD 21224. Tel.: 410-558-8202; Fax: 410-558-8150; E-mail: lakattae@mail.nih.gov.

[3] The abbreviations used are: SANC, sinoatrial nodal cells; PKA, protein kinase A; AC, adenylyl cyclase; AP, action potential; β-AR, β-adrenergic receptor; GM1, ganglioside M1; ISO, isoproterenol; NCX, Na/Ca exchanger; PDE, phosphodiesterase; SAN, sinoatrial node; q-RT, quantitative reverse transcriptase; SR, sarcoplasmic reticulum; BAPTA, 1,2-bis(2-aminophenoxy)ethane-*N*,*N*,*N*′,*N*′-tetraacetic acid.

EXPERIMENTAL PROCEDURES

Rabbit sinoatrial nodal tissue and isolated sinoatrial single nodal cells were prepared as reported previously (4).

q-RT-PCR Assays for AC Isoform Transcript Abundance—Transcript abundance of AC isoforms 1–6, 8, and 9, and soluble adenylate cyclase from rabbits were determined as previously described (13). As only full-length mRNA sequences for rabbit AC2, AC5 and soluble adenylate cyclase are available from GenBank™, primers were designed based on the most conserved motifs from human, rat, and mouse mRNA sequences for each AC. To find conserved motifs, mRNA sequences from human, rat, and mouse ACs were aligned using a program that allows local multiple alignment from Genomatix ("DiAlign"). Numerous primers were chosen and the most conserved motifs of each AC identified using the Primer3 software (13).

Each primer pair was tested using human, rat, mouse, and rabbit heart samples. Nine unique primer sets, corresponding to an individual AC (1, 2, 3, 4, 5, 6, 8, 9, soluble adenylate cyclase) (supplemental materials Table S1), yielded amplification products of appropriate sizes, except AC4, which was not analyzed further. To verify that the amplification products corresponded to appropriate ACs, fragments from rabbit intact sinoatrial node (SAN) tissue were cloned into pGEM-T Easy vector (Promega) and sequenced on ABI PRISM 310 Genetic Analyzer (PE Applied Biosystems) using SP6 and T7 promoter primers. Each sequence was analyzed using BLAST to verify its homology to the appropriate adenylate cyclase mRNA from human, rat, and mouse.

q-RT-PCR analyses were performed on AC using pre-tested primer sets. Each group tested consisted of four samples corresponding to RNA isolated from brain, SANs ($n = 3$) and SANC ($n = 3$) of individual rabbits. For q-RT-PCR, 1 μg of total RNA, previously treated with DNase I (Ambion Inc.), was reversed transcribed with random hexonucleotides (PE applied Biosystems). q-RT-PCR were run with an ABI PRISM 7900 Sequence Detector System (PE Applied Biosystems) in the presence of SYBR Green using Platinum SYBR Green qPCR SuperMix (Invitrogen). The reaction mixture (12 μl) contained 1 μl of cDNA, 6 μl of Platinum SYBR Green qPCR Super Mix-UDG, 0.2 μl of ROX reference dye, 1 μl of 10 μmol of forward and 1 μl of 10 μmol of reverse primers, and 12 μl of DNase/RNase-free water (Invitrogen). Cycling conditions were: initial denaturation at 95 °C for 2 min; 45 amplification cycles were at 95 °C for 30 s, 60 °C for 30 s, and 72 °C for 30 s. Each assay was performed in quadruplicate, and three negative controls were run for every assay: no template (sample lacking cDNA), no reverse transcriptase, and no RNA in reverse transcriptase reaction. Standard curves from cDNA dilutions of target genes and 10-fold dilutions of endogenous references (18S rRNA (18S)) were performed. The threshold cycle (Ct) of each sample was transformed to the log of the dilutions and normalized. Normalized data are presented as ($1/\Delta Ct$), where $\Delta Ct = (Ct - Ct18S)$ value (13).

Sucrose Density Gradient Fractionation of SAN Tissue and Isolated SANC—Membrane microdomain extraction and subsequent equilibrium centrifugation were performed as previously described, with only slight modifications (14). Approximately 1 mg of protein from isolated SANC was subjected to disruption in a homogenizer in 500 μl total volume of TKM buffer (50 mM Tris-HCl, pH 7.4, 25 mM KCl, 5 mM $MgCl_2$, 1 mM EDTA) + 1% Triton X-100 and protease inhibitors (2 μg/ml of each aprotinin, antipain, chymostatin, leupeptin, and trypsin inhibitor (Roche)), and extracted on ice for 30 min. The material was transferred to a SW41 centrifuge tube and mixed with an equal volume of 80% sucrose in TKM (v/v). Extracts were then gently overlaid with 6 ml of 38% sucrose/TKM, followed by 4 ml of 5% sucrose/TKM for a total volume of 11 ml. Tubes were centrifuged at 200,000 × *g* for 18 h at 4 °C in a SW41 rotor (Beckman, Fullerton, CA). Eleven 1-ml fractions were collected carefully from the top of the tube and used immediately for AC activity studies or stored at −20 °C until subsequent use. All protein concentrations were determined by BCA protein assay (Pierce).

cAMP Assay—Suspensions of intact isolated cells from a given heart were divided into control and treatment groups, consisting of 0.1 mM isobutylmethylxanthine or 1 μM isoproterenol. Aliquots of cells were incubated with gentle shaking during 5 min at 34 °C. To buffer intracellular Ca^{2+}, the same experiments were repeated with isolated cells pretreated with BAPTA-AM (25 μM) for 30 min at 34 °C.

To determine cyclic AMP levels in the isolated ventricular myocytes and SANC submitted to the different treatments, ice-cold ethanol was added to the cell suspension to have a final suspension volume of 65% ethanol. After vigorous mixing, the extracts were centrifuged at 10,000 × *g* for 15 min and 4 °C. The supernatants were collected; the remaining precipitates were washed again with ice-cold 65% ethanol and centrifuged as before. Collected supernatants were SpeedVac dried and stored at −20 °C or used immediately for cAMP measurements.

cAMP was measured by radioimmunoassay (the cAMP [^{125}I] Biotrak assay system from Amersham Biosciences (RPA 509)) as described by the manufacturer. Briefly, prior to analysis, dried extracts and standard cAMP samples were dissolved in 0.5 ml of the standard "assay buffer." The solutions were mixed with a reconstituted antiserum from a lyophilized rabbit anti-succinyl cAMP and incubated 1 h at 4 °C. The tracer, adenosine 3′,5′-cyclic phosphoric acid 2′-*o*-succinyl-3-[^{125}I]iodotyrosine methyl ester, was added to every tube, and the tubes incubated for 3 more hours at 4 °C. The secondary antibody obtained from donkey anti-rabbit serum coated onto magnetizable polymer particles was added. The mixtures were left at room temperature for 10 min, centrifuged at 2,600 × *g* and 4 °C in a Sorvall RT 6000D for 15 min. Supernatants were discarded and the tubes were inverted on absorbent pads for 5 min. The pellets were counted in a γ counter.

Adenylyl Cyclase Assay—To determine adenylyl cyclase catalytic activity of whole cells, cell suspension containing 20–50 μg of protein was precipitated and resuspended in 350 μl of lysis buffer containing 20 mM HEPES (pH 7.4), 0.1% Triton X-100, 0.5 mM dithiothreitol, and 1 μl of protease inhibitor mixture (Sigma P8340). This suspension was sonicated on ice 3 times for 30 s separated by 1 min; the sonicator setting was 3. Forty μl of this homogenate was incubated for 20 min at 30 °C in a final volume of 350 μl of an ATP regenerating system comprised of: 20 mM HEPES (pH 7.4), 0.8 mM $MgCl_2$, 0.3 mM KCl,

100 mM NaCl, 0.5 mM ATP, 5 mM creatine phosphate, 1 mM EGTA, 70 units of CPK, 0.5 mM dithiothreitol, and 0.2 mM isobutylmethylxanthine. A final [Ca^{2+}] of 0.2 or 1 μM at pH 7.4 and 30 °C was achieved by adding to the assay buffer 0.7336 or 0.9332 mM $CaCl_2$, respectively (15). At the end of the incubation the medium was extracted to determine the cAMP as described above.

A similar procedure was employed to determine AC activity in sucrose gradient-separated cell and tissue fractions. In this case, samples were 20 μl and contained ~0.8–9 μg of protein.

Immunoblots of Fractionated SAN Tissue and SANC Extracts—Dot immunoassays were performed as described previously (14), with minor modifications as outlined below. Briefly, 100-μl portions of each fraction were serially diluted and added to wells of a Bio-Dot apparatus (Bio-Rad), and incubated on nitrocellulose membranes (Millipore, 0.45 μm) for 1 h at room temperature. Gentle pressure was applied to the membrane and samples were gently suctioned, then the membrane was washed 2 times with TBST (10 mM Tris-HCl, pH 7.5, 100 mM NaCl, 0.1% Tween 20), and allowed to air dry. These membranes were then removed from the apparatus and blocked with 5% nonfat milk powder in TBST for 1 h at room temperature. Membrane strips were incubated with primary antibodies in TBST, 0.5% milk powder overnight at 4 °C and washed three times for 10 min with TBST prior to incubation with horseradish peroxidase-conjugated secondary goat anti-mouse IgG (Jackson Laboratories, Bar Harbor, ME) for 45 min. The strips were then washed three times for 15 min and developed with an enhanced chemiluminescence (ECL) assay (Amersham Biosciences) before exposure to Hyper-Film ECL (Amersham Biosciences). The following antibodies were used in dot immunoassays: AC1 and AC2 (rabbit, polyclonal), from FabGennix, Frisco, TX; AC8 (goat, polyclonal) and AC5/6 and AC-pan (rabbit, polyclonal), from Santa Cruz Biotechnology, Santa Cruz, CA; and caveolin-3 (mouse, monoclonal), from Research Diagnostic, Concord, MA. GM1 was detected by non-denatured cholera toxin, B-subunit, from Calbiochem. Densitometry was performed as previously described for Western blotting. Briefly, for blots measured on the Typhoon 9410 (GE Healthcare), ImageQuant 5.0 (GE Healthcare) was used to circle dots and measure the intensity. For measures using film (Hyperfilm, ECL, GE Healthcare), spots were measured using the freeware ScionImage (Frederick, MD). Raw intensity values were used to calculate percentage of signal intensity.

Patch Clamp Experiments on Single Isolated Rabbit SANC—A perforated patch clamp technique as described previously (16) with 50 μM β-escin (Sigma) added to the pipette solution was used to measure cell capacitance and record spontaneous APs with an Axopatch-2B patch clamp amplifier (Axon Instruments, Foster City, CA). Briefly, 35–45 μl of isolated viable rabbit SANC stored at 4 °C in KB solution were placed into the experimental chamber (total volume of 300 μl) and perfused (1.5 ml/min at 35 °C) with regular Tyrode buffer (composition (in mM): NaCl, 140; KCl, 5.4; $MgCl_2$, 1; HEPES, 5; $CaCl_2$, 1.8; glucose, 5.5; pH 7.4). The most viable regular rhythmically beating cells were utilized in the experiments. Standard electrodes with the tip resistances ranging from 3 to 4.5 MΩ filled with the standard solution containing (in mM): potassium gluconate, 120; NaCl, 10; MgATP, 5; HEPES, 5; KCl, 20 (pH 7.2), were used to obtain gigaseal and record action potentials. A subset of cells was voltage clamped to measure the hyperpolarization-activated current, I_f, in the presence and absence of CsCl (2 mM).

Pharmacological experiments employed the common AC inhibitor MDL-12,330A hydrochloride (Sigma) dissolved in water with final concentrations of 40 and 400 μM; or a specific cell permeable peptide inhibitor of the protein kinase A, PKI (Calbiochem) dissolved in water with the final concentration 15 μM; or the fast, cell-permeable Ca^{2+} chelator BAPTA-AM (Molecular Probes) dissolved in the appropriate amount of DMSO with final concentrations of 5 and 25 μM; or continuous superfusion of the cell with 2 mM CsCl to block the I_f current in spontaneously beating SANC.

RESULTS

AC mRNA Isoform Expression in SANC—AC isoforms differ in their regulation and Ca^{2+} sensitivity (17), with AC types 1 and 8 being specifically activated by Ca^{2+}. q-RT-PCR was used to determine expression levels of AC isoform RNAs in SAN tissue as well as isolated SANC. Data were compared with brain tissue in which high levels of Ca^{2+}-activated AC types have been reported (17). We observed that numerous AC isoform transcripts are expressed in SAN, in isolated SANC, and in the brain, and that relative transcript abundance for the various AC types differed widely among the three groups (supplemental materials Fig. S1). Fig. 1*A* shows representative q-RT-PCR amplifications of the AC1 isoform transcripts. Note the relatively high abundance of AC1 in brain (threshold cycle, Ct = 26) and less abundant, but definite, expression in SAN (Ct = 30) and SANC (Ct = 33). The average expression of all AC isoforms measured is illustrated in supplemental materials Fig. S1. The correct molecular weight for each transcript was observed yet each varied in abundance depending on tissue/cell type (Fig. 1, *B* and *C*). For example, AC type 5 is the dominant mRNA transcript in SAN tissue, exceeding the level in brain by 4-fold (Fig. 1*C*). The relative abundance of AC type 5 in isolated SANC is markedly less than that in SAN tissue (Fig. 1*C*). The relative abundance of AC types 1, 2, and 8 mRNA transcripts in SAN tissue is substantially lower than in brain (Fig. 1*C*), ranging from less than 1 to 8% of brain isoforms. (Note the difference in calibration of *y* axis in the *left* and *right panels* of Fig. 1*C*.) The relative mRNA abundance of types 1, 2, and 8 differ between intact SAN tissue and isolated SANC: in isolated SANC, the transcript abundance of AC type 1 is substantially less than that in SAN (by <10-fold), whereas AC type 8 transcript content is greater in SANC than in SAN.

Localization of Different AC Isoforms in Membrane Lipid Domains—The volume fraction of the caveolae of SANC exceeds, by 2-fold, that in other cardiac cell types (18). Caveolae increase the surface area of rabbit SANC external sarcolemma by 100%, whereas in rabbit papillary muscle caveolae increase the surface membrane area by only 17–27% (18). Numerous signaling pathways reside within caveolae. Because of the plasma membrane localization of ACs, the AC activity likely varies locally among membrane microdomains. Because the amino acid sequence of catalytic domains of AC families is largely conserved, the broad range of individual regulation

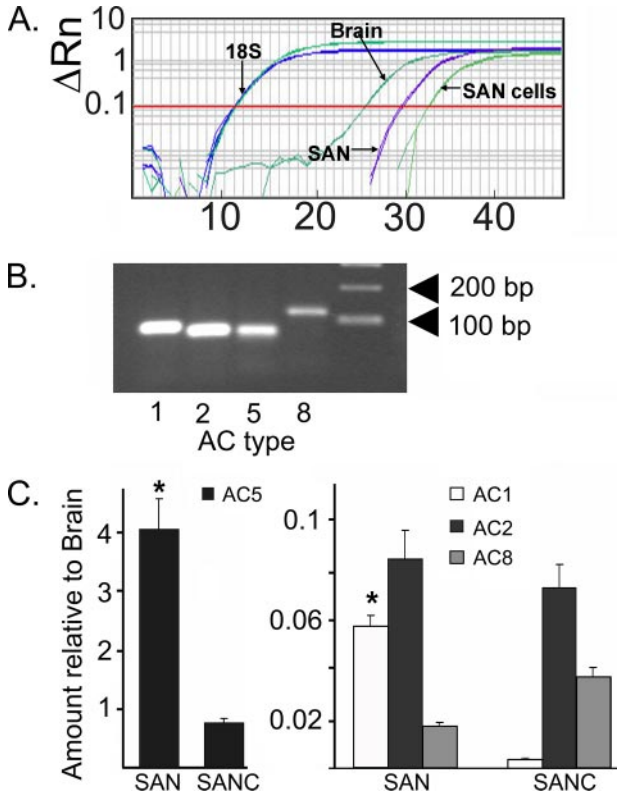

FIGURE 1. *A*, representative q-RT-PCR cycle times for 18S and AC type 1 in brain, intact SAN tissue, and isolated SANC. *B*, molecular weights of transcripts for AC isoforms 1, 2, 5, and 8. *C*, abundance of SAN ($n = 3$ hearts) or SANC ($n = 3$ hearts) AC isoform transcripts relative to brain tissues. *, significant difference in the transcript expression levels between SAN *versus* the same transcript in SANC after normalization to the brain transcript expression level (*, $p < 0.05$ (*t* test)).

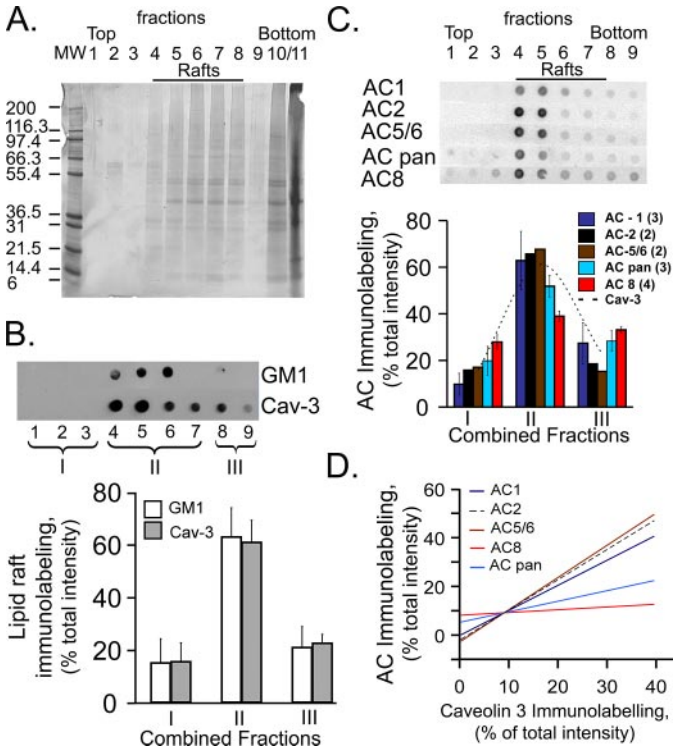

FIGURE 2. *A*, representative silver-stained gel of sucrose gradient fractions of pooled SANC from 5 isolated SAN. Buoyancy decreases as fraction numbers increase (fraction 1, most buoyant; fractions 10 and 11 more soluble fractions). *B*, *top panels* show raw data from representative immunolabeled dot blots screening for caveolin and GM1 in gels of sucrose gradient fractions. Sucrose gradient fractions shown in *panel B* have been combined into three fractions (*I–III*) as depicted in *top panel*: *fraction I* is the sum of fractions 1–3; *fraction II* it the sum of fractions 4–7; and *fraction III* is the sum of fractions 8–9. *Panel B*, *lower*, shows the average distribution of immunolabeling in each of these combined sucrose gradient fractions for caveolin-3 and GM1 in 6 experiments. *C*, *panel C*, *top*, depicts the distribution immunolabeling of AC antibody labeling; *lower panel* show the average immunolabeling. The number of experiments for each AC type is indicated in *parentheses*. *D*, representative examples of least square linear regression of relative AC isoform immunolabeling in each combined fraction, as a function of relative caveolin labeling within each fraction. r^2 and statistical significance of least squares linear regression for each AC isoforms were: AC1, $r^2 = 0.99$, $p < 0.001$; AC2, $r^2 = 0.91$, $p < 0.0001$; AC5/6, $r^2 = 0.91$, $p < 0.0001$; AC8, $r^2 = 0.46$, $p < 0.02$; AC pan, $r^2 = 0.85$, $p < 0.0001$. Similar results were observed in three additional experiments.

must be associated with the sequence diversity outside these domains (19), which may affect their binding to other molecules. Density gradient fractionation of SANC was performed and individual fractions were immunoblotted to determine relative distribution of caveolin, GM1, another lipid raft microdomain marker, and AC isoform immunolabeling. Fig. 2*A* illustrates a representative gel of 1/20 of a pooled sample of fractionated SANC isolated from five SANs. Independent fractions are labeled in each lane (fractions 1–11). Note that the buoyancy decreases as the fraction numbers increase, and that fractions 10 and 11 are the most soluble fractions.

Fig. 2*B*, *top panel*, illustrates the raw signal intensity of dot immunoblots for caveolin-3 and ganglioside M1 (GM1), a lipid raft marker depicted as a representative experiment, and the *lower panel* illustrates the average immunolabeling of three combined fractions 1–3, 4–7, and 8–9 depicted as fractions *I–III,* respectively, in the *top panel*. Note, on average 60% of caveolin and GM1 immunolabeling are located in combined fraction II. Combined fractions I and III each contain a substantially reduced, but finite immunolabeling for the lipid raft markers. Fig. 2*C* represents AC PAN and specific AC immunolabeling in a representative experiment in isolated SANC (*top*) and averaged data (*lower panel*). Although the signal intensity of most AC markers is greatest in pooled fraction II, *i.e.* the fraction containing the most intensive caveolin and GM1 immunolabeling (Fig. 2, *B* and *C*, *dashed line, lower panel*), immunolabeling of AC-PAN and AC8 across the fractions appears broader than AC 1, 2, and 5/6 antibody labeling. In new experiments, *SAN tissue,* which provides a greater protein yield than isolated SANC, was fractionated and serially diluted to probe for caveolin, GM1, and AC isoforms. Supplemental materials Fig. S2 illustrates the serially diluted immunoblots for each antibody, and supplemental Table S2 lists the relative percent signal intensity for each sample dilution in each fraction for each antibody. Note the same relative distribution of immunolabeling across the fractions for such antibody, regardless of the dilution.

Correlations between caveolin and AC immunolabeling across the fractions were high (Fig. 2*D*), suggesting that the ACs reside within lipid membrane microdomains of SANC. Differences in the slope of this relation between AC-PAN, AC8, and the other AC isoforms (Fig. 2*D*) reflect the broader immunostaining pattern of AC-PAN and AC8 (*panel D*).

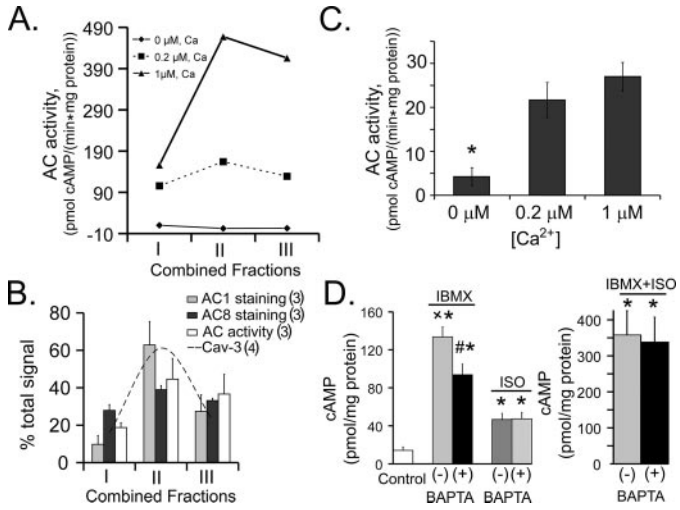

FIGURE 3. *A*, the Ca^{2+} dependence of AC activity among sucrose gradient fractions of a representative experiment of isolated SANC pooled from 5 rabbit hearts. *B*, average distribution of Ca^{2+}-activated AC isoform immunolabeling (number of experiments indicated in *parentheses*). *C*, Ca^{2+} dependence of AC activity of whole cell lysates of intact SANC isolated from SAN ($n = 6$, separate experiments, each experiment utilizing SANC from an individual heart). *D*, whole cell homogenate cAMP levels of spontaneously firing SANC following phosphodiesterase inhibition, β-AR stimulation, or a combination of both, in the presence (+) or absence (−) of chelation of intracellular Ca^{2+} by BAPTA-AM. Note the change of scale of the *y* axis in the *right versus left panel*. Cells used for each experiment were isolated from the same SAN. *, $p <$ 0.05 *versus* control; ×, $p < 0.05$ *versus* isobutylmethylxanthine (*IBMX*) (+)BAPTA; #, $p < 0.05$ *versus* IBMX or ISO alone.

AC Activity and cAMP—In isolated SANC pooled from an additional 5 hearts, total AC activity and its Ca^{2+} dependence, in addition to immunolabeling for Ca^{2+}-activated ACs in each fraction depicted in Fig. 2, *B* and *C*, was measured. Fig. 3*A* indicates a marked Ca^{2+} dependence of basal AC activity over the physiologic intracellular Ca^{2+} range (0.2–1 μM). Note that most of the Ca^{2+} activation of AC activity lies within combined fractions II and III. Note also that in the absence of Ca^{2+} AC activity drops to nearly undetectable levels. Fig. 3*B* illustrates the average relative distributions of Ca^{2+}-activated AC activity and Ca^{2+}-activated AC isoform immunolabeling. On average, 80% of AC activity was detected in fractions II and III with 20% in fraction I. The relative distribution of AC activity among the three fractions generally parallels that of Ca^{2+}-activated AC isoform immunolabeling. The different profiles of AC1 and AC8 immunolabeling is noteworthy: AC type 1 immunolabeling tracks that of caveolin (Fig. 2*C*, *dashed line*) with 60% of it being localized within fraction II; AC type 8 immunolabeling has a broader distribution across the fractions with 40% being present in fraction II and 30% found in each of the other type of fractions, *i.e.* more similar to the distribution of Ca^{2+}-activated AC activity.

Fig. 3*C* provides direct evidence, in whole cell lysates of intact SANC, of Ca^{2+}-stimulated AC activity in the absence of sucrose density cell fractioning. Following incubation of whole cell lysates in Ca^{2+}-free buffer containing EGTA, AC activity was greatly increased by incubation in the presence of Ca^{2+} at concentrations that occur within the physiologic range in intact cells.

In *intact*, isolated SANC, Ca^{2+} buffering, PDE inhibition, or β-AR stimulation markedly affect the cAMP level (Fig. 3*D*). PDE inhibition increases the basal cAMP level by 9-fold, exposing a high level of AC activity (Fig. 3*D*, *left panel*). This cAMP increase in the presence of PDE inhibition is reduced by 30% by chelation of intracellular Ca^{2+} with BAPTA. Fig. 3*D*, *left panel*, shows that β-AR stimulation with isoproterenol (ISO) increases the cAMP level, but to a markedly lesser extent than PDE inhibition. Furthermore, the ISO-induced increase in cAMP is not reduced by Ca^{2+} buffering. The combination of ISO and PDE inhibition (Fig. 3*D*, *right panel*), however, increases cAMP to a level that substantially exceeds (by 7-fold) that induced by ISO alone (note difference in *ordinate scale* in *left* and *right panels*). This suggests that PDE activity, in addition to regulating the basal cAMP, also moderates the increasing cAMP level regulated by ACs that are activated by β-ARs. Still, unlike PDE inhibition alone, the combined ISO plus PDE-induced increase in cAMP is not reduced by intracellular Ca^{2+} buffering.

Effects of Inhibition of Adenylyl Cyclase, PKA, or Ca^{2+} Buffering on Spontaneous AP Firing in Isolated SANC—Numerous interacting subcellular mechanisms link Ca^{2+} activation AC activity, cAMP, cAMP-dependent phosphorylation of ion channels, and Ca^{2+} itself to pacemaker cell function. Fig. 4*A* illustrates a schematic of the potential interplay between Ca^{2+}, AC, cAMP-PKA signaling, SR Ca^{2+} cycling proteins, and ion sarcolemmal ion channels. We employed pharmacological measurements in an attempt to partially sort the functional implications of some of these interactions.

The dependence of spontaneous AP generation on intracellular Ca^{2+} (Fig. 4*A*) is clearly demonstrated by the ability of intracellular Ca^{2+} chelating by BAPTA-AM to abrogate spontaneous AP firing (Fig. 4*B*). This effect of Ca^{2+} buffering could occur via a reduced Ca^{2+} activation of AC (Fig. 3, *C* and *D*, *left panel*), leading to a local [cAMP] reduction (Fig. 4*A*), as MDL, an AC inhibitor, also abrogates spontaneous AP firing (Fig. 4*C*).

A change in I_f an ion current formed by the combination of HCN subunits having cAMP binding elements is likely sequela of a change in cAMP. Complete inhibition of the I_f current by 2 mM CsCl, however (Fig. 4*D*), has only a modest effect to reduce spontaneous AP firing. A change in cAMP resulting from a change in AC activity, also induces downstream, cAMP-mediated, PKA-dependent phosphorylation of ion channels, *e.g.* $I_{Ca,\,L}$, of SR Ca^{2+} cycling proteins, *e.g.* phosphorylation of phospholamban and ryanodine receptors (Fig. 4*A*), that control the cell and SR Ca^{2+} loading and Ca^{2+} release. Fig. 4*E* shows that this distal cAMP pathway signaling is crucial to pacemaking function, as PKI, a specific peptide inhibitor of PKA, abrogates SANC AP firing.

DISCUSSION

Our results show that: 1) rabbit SANC express two Ca^{2+}-activated AC isoforms in addition to other non-Ca^{2+}-activated AC isoforms; 2) AC immunolabeling is largely confined to membrane lipid microdomains; 3) virtually all basal AC activity is Ca^{2+}-activated and the majority of Ca^{2+} activation of AC activity occurs within lipid raft microdomains containing specific lipid raft markers caveolin and GM1; 4) the basal cAMP level and that following β-ARs stimulation are restricted by high basal PDE activity; 5) that the high basal cAMP levels in

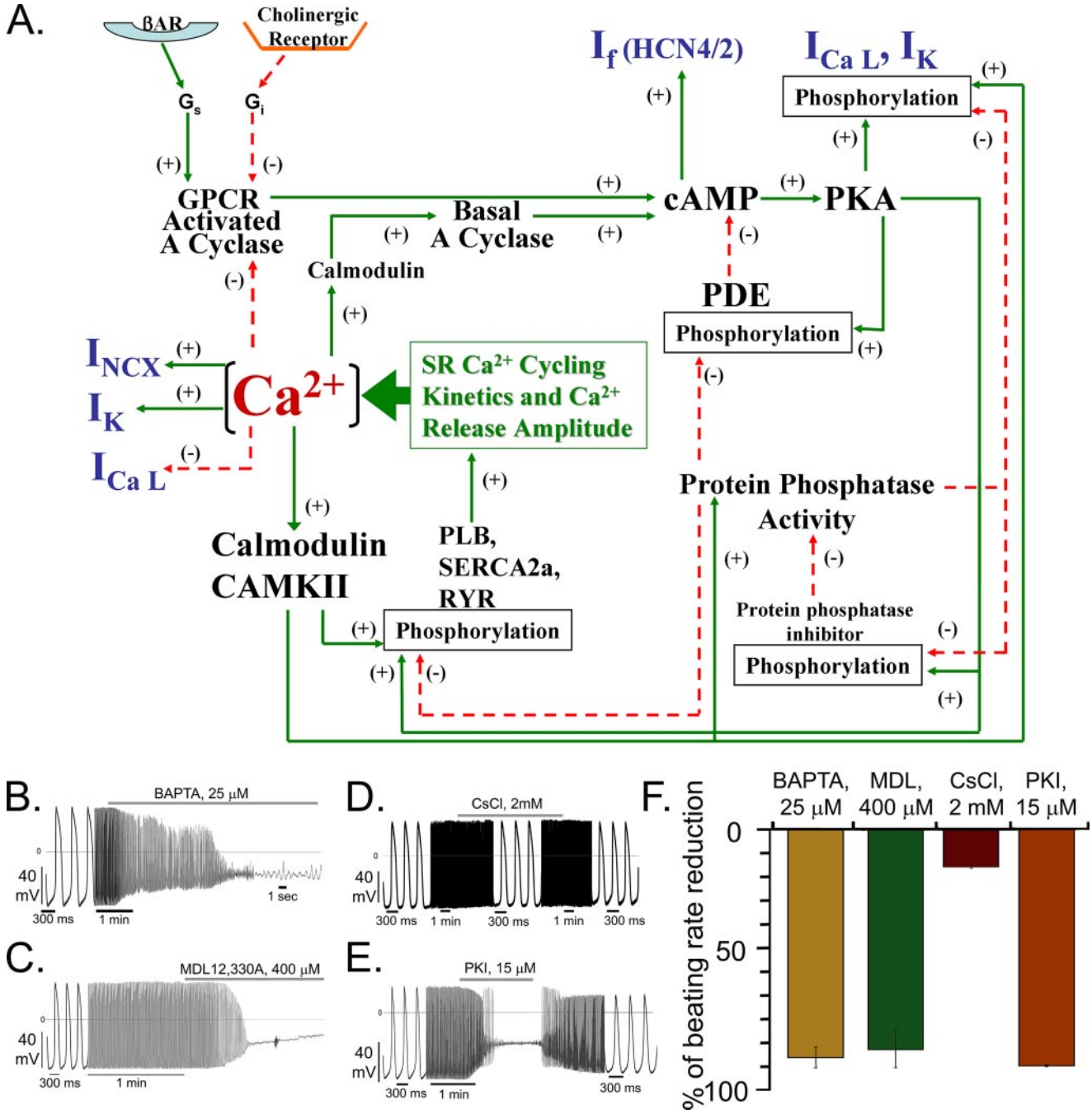

FIGURE 4. *A*, schematic illustration of the interplay of Ca^{2+}, basal Ca^{2+}-activated AC, cAMP, PDE activity, and PKA activity, cast in the context of sarcoplasmic reticulum Ca^{2+} cycling, L-type Ca^{2+} channels, and other ion channels. Ca^{2+} activation of NCX initiates, in turn, spontaneous SANC APs, as reported previously (2–10). Ca^{2+} activation of basal AC activity results in a feed forward "fail safe" system to generate cAMP and cAMP/PKA-dependent phosphorylation. Ca^{2+} cycling protein phosphorylation (phospholamban, ryanodine receptors, L-type Ca^{2+} channels, and cross-talk of these) generates both local, spontaneous submembrane Ca^{2+} releases, and global increases in cytoplasmic Ca^{2+} triggered by APs activate ACs. Ca^{2+}, cAMP, or PKA-dependent phosphorylation also modulates other ion channels. The dual basal Ca^{2+}/cAMP-PKA "feed forward regulation" is kept in check by a high basal PDE activity, which prevents cAMP/PKA signaling to become excessive, *i.e.* acts as negative feedback mechanism to prevent an excessive basal beating rate, and to ensure reserve cAMP/PKA modulation of spontaneous beating via activation of β-ARs. Phosphatase activity likely constitutes an additional intrinsic brake on PKA signaling in SANC but this has not yet been measured. Note that because the cAMP increase induced by β-AR stimulation is not reduced by Ca^{2+} chelation (Fig. 3*D*) the ACs that couple to β-ARs (and associated PDEs) are depicted in the scheme in a separate location from the basal Ca^{2+}-activated ACs. *B*, the effects of Ca^{2+} chelation, AC inhibition, I_f blockade, or PKA inhibition on spontaneous SANC AP firing rate. Representative examples of: *B*, chelation of intracellular Ca^{2+} by 25 μM cell permeable fast Ca^{2+} chelator BAPTA-AM ($n = 6$); *C*, AC inhibition by 400 μM MDL-12,330A ($n = 5$); *D*, I_f blockade by 2 mM CsCl ($n = 7$); *E*, PKA inhibition by 15 μM PKI ($n = 5$), a specific inhibitory peptide of PKA. *F*, the average maximum effect of BAPTA-AM, MDL-12330A, PKI, or CsCl on the spontaneous AP firing rate in rabbit SANC.

SANC are, in part, produced by Ca^{2+}-activated ACs sensitive to intracellular Ca^{2+} buffering, whereas the increase in cAMP following β-AR stimulation is not; and 6) in intact isolated spontaneously beating cells, intracellular Ca^{2+} buffering or inhibition of AC activity or PKA activation preclude spontaneous AP firing.

Mammalian ACs are comprised of a set of nine isoforms (17). Types 5 and 6 are the major isoforms in the heart ventricle and atria; type 5 is predominantly expressed in adult cardiac tissues and type 6 in fetal cardiac tissues (20). Ca^{2+}-calmodulin-activated types 1 and 8 have previously been thought to be expressed exclusively in neuronal tissues (21). A recent report, however, provided evidence that the AC1 isoform is expressed in guinea pig SAN (11). Our q-RT-PCR results demonstrate that both rabbit SAN and SANC express multiple AC isoform mRNA transcripts, the most abundant of which is AC type 5 (supplemental materials Fig. S1). In addition, SAN and SANC also express transcripts for Ca^{2+}-activated AC isoforms types 1 and 8, but at levels substantially less than in brain (Fig. 1).

The present results demonstrate that AC isoforms and Ca^{2+}-dependent AC activity largely reside within SANC caveolin-enriched membrane microdomains (Fig. 2). Microdomain Ca^{2+} levels likely regulate Ca^{2+}-activated ACs (isoforms 1 and 8) that reside within these lipid raft microdomains. It is noteworthy that ryanodine receptor and other Ca^{2+} cycling proteins such as NCX and L-type Ca^{2+} channels that drive spontaneous beating of SANC (1) and HCN proteins that form the channels that carry I_f (22) also reside in these caveolin-rich lipid microdomains (23–27).

Numerous studies in other cell types (28–31) have demonstrated AC localization within caveolin-rich lipid microdomains. Ca^{2+}-activated AC types have also been localized to caveolin microdomains containing store-operated Ca^{2+}-operated Ca^{2+} channels (32). Although there is presently no evidence for functional store-operated Ca^{2+} channels in rabbit SANC, recent evidence suggests that these channels are present in mouse SAN tissue (33).

A high basal PDE activity in SANC has recently been demonstrated (10). The present results show that both Ca^{2+}-activated AC activity (Fig. 3*C*) within lipid rafts (Fig. 3*B*), and PDE activity (Fig. 3*D*) regulate basal cAMP levels in SANC. A high basal AC activity coupled to high PDE activity creates continuous cAMP synthesis and degradation. It has been proposed that restricting such continuous cAMP production and degradation to subcellular components would be an energetically efficient way to allow a system (*e.g.* light adapted photoreceptor cells (34) or cyclic nucleotide-gated channels (35)) to respond rapidly to a stimulus. The ability to effect rapid changes in heart rate confers a distinct survival and cardiovascular homeostatic benefit. If PDEs were localized to the vicinity of ACs within SANC rapid local cAMP production and degradation would continuously occur. This would permit rapid changes in the beating rate in response to changes in basal Ca^{2+}, which regulates the AC arm of the AC-PDE dual control (Fig. 4*A*). In this regard it is noteworthy that overexpression of AC type 8 in mice results in both a constitutively active, Ca^{2+}-calmodulin AC type 8 activity (36) and increased activity of the Ca^{2+}-calmodulin-activated type 1 PDE toward cAMP (37) which, in turn, leads to an elevated basal heart rate in the absence of vagal tone (38).

β-ARs are known to activate the 5/6 AC isoforms. Interestingly, our results (Fig. 3*D*) show that the cAMP increase following β-AR stimulation by ISO is not reduced by Ca^{2+} chelation, suggesting that β-AR AC activation occurs in a microdomain that is distinct from Ca^{2+}-activated ACs that regulate basal cAMP. Furthermore, one or more PDE isoforms may localize to the β-AR-AC 5/6 microdomain, because PDE inhibition markedly elevates the ISO-induced cAMP elevation (Fig. 3*D*). The dual Ca^{2+} "feed forward" regulation of cAMP, kept in check by a high basal PDE activity (Fig. 4*A*), *i.e.* a negative feedback mechanism, to prevent an excessively high basal cAMP, and to ensure reserve function in response to activation of β-AR stimulation.

The basal cAMP level is crucial to spontaneous AP firing of SANC because AC inhibition can abrogate spontaneous firing (Fig. 4*C*) (2, 11). The effect of MDL appears to be largely attributable to inhibition of Ca^{2+}-activated adenylyl cyclases (Fig. 4*A*) as prior intracellular Ca^{2+} buffering markedly reduces the effectiveness of MDL to inhibit the cAMP-dependent ionic current (11). There are numerous specific links between basal cAMP regulation and spontaneous AP firing by SANC. cAMP modulation of the hyperpolarization activated current I_f is one such potential mechanism. A most obvious target of cAMP is the HCN4 ion channel subunits that predominantly generate I_f current in pacemaker cells (Fig. 4*A*). It is well documented, in fact, that cAMP binding to I_f channels shifts I_f activation I–V curve enabling an increased current at a given voltage (39). Although cAMP-modulated gating of I_f causes a statistically significant reduction in the spontaneous firing rate in isolated rabbit pacemaker cells, this effect is minor (Fig. 4*D*). In hearts of embryonic lethal (40) HCN4 knock-out mice the beating rate is reduced by 25–50%, and conditional knock-out of HCN4 at a later age results in an irregular heart rhythm (41). Pharmacologic I_f blockade (42, 43), rather than ionic blockade, results in slowed or dysrhythmic AP firing in wild type mouse cells (44).

The effects of either intracellular Ca^{2+} chelation (Fig. 4*B*) or AC inhibition by MDL (Fig. 4*C*) to abrogate spontaneous AP firing could be attributable, in part at least, to a reduction in PKA-dependent phosphorylation modulation of surface membrane ion channels or to reduced PKA-dependent phosphorylation in SR Ca^{2+} cycling proteins (Fig. 4*A*). Indeed, a specific PKA peptide inhibitor blocks spontaneous firing (Fig. 4*E*). Prior studies have shown that PKI or MDL each inhibit phospholamban phosphorylation in a dose-dependent manner (2) that correlates with their dose-dependent effects to reduce spontaneous AP firing of SANC.

In summary, SANC express both Ca^{2+}-activated and other AC isoforms, and exhibit a high Ca^{2+}-dependent basal activation of ACs that occurs largely within membrane lipid microdomains. Given the profile of the effects of pharmacologic interventions to reduce or abrogate spontaneous firing we favor the interpretation that the local basal Ca^{2+} cycling regulates AC-driven, cAMP-mediated, PKA-dependent phosphorylation of Ca^{2+} cycling proteins that results in rhythmic local Ca^{2+} releases that drive the generation of rhythmic action potentials. At the present time, however, there is no evidence that local Ca^{2+} oscillations also produce local, beat to beat oscillations in cAMP (45), or that beat to beat changes in cAMP-mediated PKA-dependent phosphorylation within SANC are crucial to the pacemaker function.

Acknowledgments—We thank Drs. Magdalena Juhaszova and Steven Sollott for helpful suggestions.

REFERENCES

1. Maltsev, V. A., Vinogradova, T. M., and Lakatta, E. G. (2006) *J. Pharmacol. Sci.* **100,** 338–369
2. Vinogradova, T. M., Lyashkov, A. E., Zhu, W., Ruknudin, A. M., Sirenko, S., Yang, D., Deo, S., Barlow, M., Johnson, S., Caffrey, J. L., Zhou, Y. Y., Xiao, R. P., Cheng, H., Stern, M. D., Maltsev, V. A., and Lakatta, E. G. (2006) *Circ. Res.* **98,** 505–514
3. Lyashkov, A. E., Juhaszova, M., Dobrzynski, H., Vinogradova, T. M., Maltsev, V. A., Juhasz, O., Spurgeon, H. A., Sollott, S. J., and Lakatta, E. G. (2007) *Circ. Res.* **100,** 1723–1731
4. Bogdanov, K. Y., Vinogradova, T. M., and Lakatta, E. G. (2001) *Circ. Res.* **88,** 1254–1258
5. Maltsev, V. A., Vinogradova, T. M., Bogdanov, K. Y., Lakatta, E. G., and Stern, M. D. (2004) *Biophys. J.* **86,** 2596–2605
6. Sanders, L., Rakovic, S., Lowe, M., Mattick, P. A., and Terrar, D. A. (2006) *J. Physiol.* **571,** 639–649
7. Vinogradova, T. M., Zhou, Y. Y., Maltsev, V., Lyashkov, A., Stern, M., and Lakatta, E. G. (2004) *Circ. Res.* **94,** 802–809
8. Bogdanov, K. Y., Maltsev, V. A., Vinogradova, T. M., Lyashkov, A. E., Spurgeon, H. A., Stern, M. D., and Lakatta, E. G. (2006) *Circ. Res.* **99,** 979–987
9. Vinogradova, T. M., Bogdanov, K. Y., and Lakatta, E. G. (2002) *Circ. Res.* **90,** 73–79
10. Vinogradova, T. M., Sirenko, S., Lyashkov, A. E., Younes, A., Li, Y., Zhu, W., Yang, D., Ruknudin, A. M., Spurgeon, H., and Lakatta, E. G. (2008) *Circ. Res.* **102,** 761–769
11. Mattick, P., Parrington, J., Odia, E., Simpson, A., Collins, T., and Terrar, D. (2007) *J. Physiol.* **582,** 1195–1203
12. Vinogradova, T. M., Ruknudin, A. M., Zhu, W., Lyashkov, A. E., Volkova, M. V., Boheler, K. R., Xiao, R. P., Spurgeon, H. A., and Lakatta, E. G. (2006) *Biophys. J.* **90,** 155a
13. Tarasova, Y. S., Riordon, D. R., Tarasov, K. V., and Boheler, K. R. (2006) *Embryonic Stem Cells: A Practical Approach*, Oxford University Press, New York
14. Ilangumaran, S., Arni, S., Chicheportiche, Y., Briol, A., and Hoessli, D. C. (1996) *Anal. Biochem.* **235,** 49–56
15. Bers, D. M., Patton, C. W., and Nuccitelli, R. (1994) *Methods Cell Biol.* **40,** 3–29
16. Vinogradova, T. M., Zhou, Y. Y., Bogdanov, K. Y., Yang, D., Kuschel, M., Cheng, H., and Xiao, R. P. (2000) *Circ. Res.* **87,** 760–767
17. Hanoune, J., and Defer, N. (2001) *Annu. Rev. Pharmacol. Toxicol.* **41,** 145–174
18. Masson-Pevet, M., Bleeker, W. K., and Gros, D. (1979) *Circ. Res.* **45,** 621–629
19. Taussig, R., and Gilman, A. G. (1995) *J. Biol. Chem.* **270,** 1–4
20. Tobise, K., Ishikawa, Y., Holmer, S. R., Im, M. J., Newell, J. B., Yoshie, H., Fujita, M., Susannie, E. E., and Homcy, C. J. (1994) *Circ. Res.* **74,** 596–603
21. Cali, J. J., Zwaagstra, J. C., Mons, N., Cooper, D. M., and Krupinski, J. (1994) *J. Biol. Chem.* **269,** 12190–12195
22. Barbuti, A., Gravante, B., Riolfo, M., Milanesi, R., Terragni, B., and DiFrancesco, D. (2004) *Circ. Res.* **94,** 1325–1331
23. Balijepalli, R. C., Foell, J. D., Hall, D. D., Hell, J. W., and Kamp, T. J. (2006) *Proc. Natl. Acad. Sci. U. S. A.* **103,** 7500–7505
24. Bossuyt, J., Taylor, B. E., James-Kracke, M., and Hale, C. C. (2002) *FEBS Lett.* **511,** 113–117
25. Liu, L., Mohammadi, K., Aynafshar, B., Wang, H., Li, D., Liu, J., Ivanov, A. V., Xie, Z., and Askari, A. (2003) *Am. J. Physiol.* **284,** C1550–C1560
26. Lohn, M., Furstenau, M., Sagach, V., Elger, M., Schulze, W., Luft, F. C., Haller, H., and Gollasch, M. (2000) *Circ. Res.* **87,** 1034–1039
27. Scriven, D. R., Klimek, A., Asghari, P., Bellve, K., and Moore, E. D. (2005) *Biophys. J.* **89,** 1893–1901
28. Head, B. P., Patel, H. H., Roth, D. M., Lai, N. C., Niesman, I. R., Farquhar, M. G., and Insel, P. A. (2005) *J. Biol. Chem.* **280,** 31036–31044
29. Head, B. P., Patel, H. H., Roth, D. M., Murray, F., Swaney, J. S., Niesman, I. R., Farquhar, M. G., and Insel, P. A. (2006) *J. Biol. Chem.* **281,** 26391–26399
30. Schwencke, C., Yamamoto, M., Okumura, S., Toya, Y., Kim, S. J., and Ishikawa, Y. (1999) *Mol. Endocrinol.* **13,** 1061–1070
31. Swaney, J. S., Patel, H. H., Yokoyama, U., Head, B. P., Roth, D. M., and Insel, P. A. (2006) *J. Biol. Chem.* **281,** 17173–17179
32. Fagan, K. A., Mahey, R., and Cooper, D. M. (1996) *J. Biol. Chem.* **271,** 12438–12444
33. Ju, Y. K., Chu, Y., Chaulet, H., Lai, D., Gervasio, O. L., Graham, R. M., Cannell, M. B., and Allen, D. G. (2007) *Circ. Res.* **100,** 1605–1614
34. Nikonov, S., Lamb, T. D., and Pugh, E. N., Jr. (2000) *J. Gen. Physiol.* **116,** 795–824
35. Rich, T. C., Tse, T. E., Rohan, J. G., Schaack, J., and Karpen, J. W. (2001) *J. Gen. Physiol.* **118,** 63–78
36. Georget, M., Mateo, P., Vandecasteele, G., Jurevicius, J., Lipskaia, L., Defer, N., Hanoune, J., Hoerter, J., and Fischmeister, R. (2002) *FASEB J.* **16,** 1636–1638
37. Georget, M., Mateo, P., Vandecasteele, G., Lipskaia, L., Defer, N., Hanoune, J., Hoerter, J., Lugnier, C., and Fischmeister, R. (2003) *FASEB J.* **17,** 1380–1391
38. Lipskaia, L., Defer, N., Esposito, G., Hajar, I., Garel, M. C., Rockman, H. A., and Hanoune, J. (2000) *Circ. Res.* **86,** 795–801
39. DiFrancesco, D., and Tortora, P. (1991) *Nature* **351,** 145–147
40. Stieber, J., Herrmann, S., Feil, S., Loster, J., Feil, R., Biel, M., Hofmann, F., and Ludwig, A. (2003) *Proc. Natl. Acad. Sci. U. S. A.* **100,** 15235–15240
41. Herrmann, S., Stieber, J., Stockl, G., Hofmann, F., and Ludwig, A. (2007) *EMBO J.* **26,** 4423–4432
42. Bucchi, A., Baruscotti, M., and DiFrancesco, D. (2002) *J. Gen. Physiol.* **120,** 1–13
43. DiFrancesco, D. (2005) *Curr. Med. Res. Opin.* **21,** 1115–1122
44. Stieber, J., Wieland, K., Stockl, G., Ludwig, A., and Hofmann, F. (2006) *Mol. Pharmacol.* **69,** 1328–1337
45. Zaccolo, M., and Pozzan, T. (2003) *Trends Neurosci.* **26,** 53–55